JOURNAL OF GUIDANCE, CONTROL, AND DYNAMICS
Vol. 31, No. 5, September–October 2008

Guidance Algorithm for Range Maximization and Time-of-Flight Control of a Guided Projectile

Craig A. Phillips*
Naval Surface Warfare Center, Dahlgren, Virginia 22448

DOI: 10.2514/1.31327

The availability of gun-hardened guidance and control systems has made highly accurate gun-launched rocket-assisted guided projectiles feasible. A composite guidance algorithm is presented for such vehicles. The algorithm is capable of extending range and cross-range capability of the projectile, and allows it to be retargeted after launch. The algorithm also employs model predictive control to control time of flight to allow a salvo of projectiles to arrive simultaneously. The time-of-flight control achieves its objective by trajectory shaping and corrects for winds, off-nominal launch conditions, and rocket motor variations.

I. Introduction

TECHNOLOGIES for highly accurate projectile guidance such as gun-hardened Global Positioning System (GPS) receivers and microelectromechanical system (MEMS) electronic packages provide a new type of mission for projectiles. After the initial gun launch to a high speed, a rocket motor is fired during the ascent phase to further increase specific energy. This is followed by a range extension gliding portion after the ballistic apogee. The glide portion dictates the need for active control with lifting surfaces which may be employed at any point during the ascent. The projectile must be able to provide simultaneous arrival for maximum salvo lethality. The limited rate of fire of guns places a requirement for the time-of-flight (ToF) control of the projectile to satisfy this multiple simultaneous round (MSR) requirement. This time-of-flight control must account both for known variations, such as the planned salvo firing rate, and unknown variations that occur in-flight. The planned variations may be compensated by the fire control trajectory parameter selection. The in-flight variations, such as winds, muzzle velocity variations, and drag variations, require an active in-flight algorithm for their correction. The goals of absolute range maximization and time-of-flight control are in conflict and, as such, the span of target ranges at which the MSR requirement may be achieved is restricted to a subset of the feasible span of ranges for the projectile.

The design of a practical mission for a guided projectile is a complex problem that is severely constrained by a large number of operational issues, and the goal of which is to optimize performance in terms of complex relationships between the projectile, its payload, the environment, the intended target, and politically driven mission constraints. These relationships are not readily definable in a mathematically tractable way. The mission design necessarily includes trajectory design at its core and the trajectory may need to operate very near its constraints to maximize performance. The goal of the present paper is to provide a process by which the designer can rapidly trade off trajectory shaping to optimize multi-objective mission goals within a set of complex constraints.

The processes for optimization of trajectories fall into two broad approaches. The first is the optimal control methodology, which yields a two-point boundary value problem. The resulting problem can be solved numerically using an open-loop solution, or the problem can be approximated by a reduced-order model which is used to determine the corresponding closed-loop analytical guidance. Although this method yields an implementable algorithm, it involves approximations which may limit its applicability. The other broad approach is parameter optimization. In this approach, the optimal control is approximated by an optimal finite set of parameters. The resulting open-loop control may be difficult to directly implement in a real-time system, but can provide insight during the airframe design phase.

The homing of guided missiles against single targets has been extensively studied. Proportional navigation laws have been proposed for three-dimensional engagements and the miss distances of missiles guided by these laws due to target maneuvers, heading errors from midcourse phase navigation errors, receiver noise, and radom aberrations have been presented [1–6]. These efforts have yielded both numerical and closed-form solutions. The proportional navigation laws provide a small miss distance against either a fixed target or a moving target, but do not provide control over the final velocity orientation. The proportional navigation laws have typically been developed with significant assumptions, such as linearity and constant velocity, which may limit their use in certain applications to relatively short segments of the trajectory such as the end game.

Guidance laws that maneuver a weapon from its current position to a desired final position while controlling the orientation of the final velocity have been developed under the general term of explicit guidance. The original version of explicit guidance is due to Cherry [7] and is further explored in [8,9]. Other guidance methods that attempt to control both miss distance and terminal geometry have been proposed in [10–19].† It is possible to derive a generalized form of explicit guidance (see [15,17]) in which the cost function to be minimized is itself specified in terms of a user-defined parameter. This parameter, along with the initial and final flight-path angles, becomes a design parameter that the user may adjust to achieve a particular performance. As with the proportional navigation, significant assumptions are made in the development of these laws which may restrict their use in some applications.

The equations of motion associated with flight vehicle dynamics are highly nonlinear and require complex aerodynamic and propulsion force models. To overcome these complications, simplified analysis models based on quasi-steady approximations have been employed. One such method is the energy-state approximation assuming quasi-steady equilibrium glide at constant dynamic pressure, which provides that flying at maximum lift-to-drag ratio maximizes the gliding range of the vehicle. Examples of applications of the stick-fixed maximum lift-to-drag ratio flight can

Presented at the Missile Sciences Conference, Monterey, CA, 14 November 2006; received 30 March 2007; accepted for publication 4 January 2008.

*Section Head, Unmanned Systems Integration Branch, G82, 17320 Dahlgren Road, Associate Fellow.

†Menon, P. K., and Ohlmeyer, E. J., "Integrated Guidance-Control Systems for Fixed-Aim Warhead Missiles," ADA386510, URL: http://www.optisyn.com/research/papers/papers/2000/MSCd2000.pdf [cited 7 Nov. 2000].

be found in [20,21]. Analysis has indicated that nonsteady cruise solutions may produce fuel-optimal performance greater than that obtained for steady cruise [22]. In a similar fashion, investigations have been conducted into maximizing range performance for gliding vehicles by providing a near-equilibrium glide where a near-phugoid-like motion is controlled via the guidance algorithm. Kelley et al. [23] present an algorithm that provides a design parameter to control the flight-path angle between a steady dynamic pressure glide with feedforward anticipation of the specific energy loss in the glide angle and the stick-fixed (at maximum lift-to-drag) trajectory with the natural phugoid motion. The resulting trajectory lies in the range in between these cases, and the reference demonstrates that the trajectory produces range performance in excess of either of the two extremes. Lu [24] provides a rigorous examination of near-equilibrium glide in entry flight of a gliding flight vehicle. The energy model methods are unable to accommodate all of the boundary conditions, such as the final position and final velocity conditions, without some type of correction or blending.

The singular perturbation methods developed as an attempt to recover, in at least an approximate sense, the faster dynamics required to achieve these boundary conditions. Naidu and Calise [25] provide an overview of the singular perturbation methods for the guidance and control problem. The singular perturbation methods often require real-time numerical solution of the resulting two-point boundary value problem. For the cruise or gliding vehicle, the *outer* solution determined in singular perturbation methods is similar to the solution found from the energy modeling methods.

An alternative numerical-based technique to maximize performance while meeting terminal constraints is the *Optimal-Path-to-Go* algorithm, which employs an online optimal trajectory algorithm [26]. In this method, an online database of previously developed optimal trajectories is encoded and interrogated online at regular intervals. The current vehicle states are used as input to the algorithm to generate the optimal guidance commands to the desired terminal states. These trajectory commands are used over the next trajectory segment, at which point they are updated.

The model predictive control (MPC) approach provides a method for feedback control for nonlinear systems where the dynamics are slow relative to the computational update rate. In model predictive control, a nonlinear simulation of the system projects the states onto a future receding horizon or fixed terminal horizon and uses the estimated states at the horizon to determine the control action. The method is used in industrial control, but the advent of fast computer processing for onboard vehicle use has made it a candidate for controlling the slower processes on flight vehicles, such as the total time of flight to the target. A model predictive control strategy for a parafoil aircraft has been reported [27].

The contribution of the present paper is to provide a framework for creating a composite guidance algorithm for combining the near-equilibrium glide management algorithm of [23], the vectorized three-dimensional version of the explicit algorithm of [15,17], with a model process control approach for the control of time of flight to allow multiple simultaneous round impact for a boost glide vehicle. The framework allows the selection of a relatively few parameters by the designer to control the trajectory and mission to achieve complex nontractable performance goals across the battlespace.

II. Algorithm Overview

The algorithm produces a composite guidance acceleration expressed in the North, East, down at launch (NEDL) frame composed of three terms.

$$\bar{a}^{\,\mathrm{NEDL}} = \sum_{i=1}^{3} \bar{a}_i^{\mathrm{NEDL}} \tag{1}$$

The first is the homing guidance algorithm that ensures that the missile flies to the target and arrives with a selected velocity orientation. The second term is a bias for cancellation of the gravity acceleration and for in-flight time-of-flight control. The function of the third term is to fly the projectile along an optimal flight path to conserve energy. The relative weighting of the components of the acceleration command are scheduled during the flight.

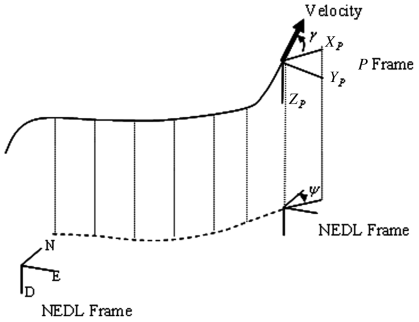

Fig. 1 *P* frame definition.

The weighting of the individual components of the composite algorithms are critical. Two of the components are best defined in terms of the *P* frame (see Fig. 1). These are the energy management and the time-of-flight controls. The *P* frame is the Earth local tangent frame at the missile position with its *x* axis aligned with the missile's current bearing (the projection of the missile velocity onto the local tangent plane). The *z* axis of the *P* frame points along the local gravity vector.

The relative weighting of the components is naturally done in the vertical plane defined by the *x*-*z* axes of the *P* frame. Thus, the weighting factor scheduling is done in the *P* frame. From [15,17], the homing component was defined in the NEDL frame. Its component must be transformed into the *P* frame for weighting. The resulting composite law expressed finally in the NEDL frame is given by

$$\bar{a}^{\mathrm{NEDL}} = T_{P2\mathrm{NEDL}}\tilde{K}_{\mathrm{dsm}}T_{P2\mathrm{NEDL}}^{T}\bar{a}_{\mathrm{exp}}^{\mathrm{NEDL}} + T_{P2\mathrm{NEDL}}\tilde{K}_{\mathrm{dsm}}\bar{a}_{\mathrm{bias}}^{P} + (\mathbf{I} - \tilde{K}_{\mathrm{dsm}})T_{P2\mathrm{NEDL}}\bar{a}_{\mathrm{em}}^{P} \tag{2}$$

$T_{P2\mathrm{NEDL}}$ is the transformation from the *P* frame to the NEDL frame. For the flat Earth, this transformation is created through a rotation of the current azimuthal angle of the current missile velocity. The homing element of the acceleration command expressed in the NEDL frame is $\bar{a}_{\mathrm{exp}}^{\mathrm{NEDL}}$. The energy management acceleration component expressed in the *P* frame is $\bar{a}_{\mathrm{em}}^{P}$. The bias command for time-of-flight control and gravity bias correction expressed in the *P* frame is $\bar{a}_{\mathrm{bias}}^{P}$.

$\tilde{K}_{\mathrm{dsm}}$ is a gain tensor of the form $\begin{bmatrix} K_{\mathrm{dsm}} & 0 & 0 \\ 0 & 1 & 0 \\ 0 & 0 & K_{\mathrm{dsm}} \end{bmatrix}$

The purpose of the gain tensor is to allow the shaping in the vertical plane defined by the *x*-*z* axes of the *P* frame to be controlled, while allowing the homing commands normal to this plane to be unrestricted. The value of the scalar K_{dsm} is selected based on the value of the range-to-go (RGO) (in feet) to the target.

$$\begin{aligned} &\text{IF RGO} \geq \mathrm{RGO}_M\text{: } K_{\mathrm{dsm}} = 0 \\ &\text{IF } \mathrm{RGO}_M > \mathrm{RGO} > \mathrm{RGO}_M - 5000.\text{: } K_{\mathrm{dsm}} = (\mathrm{RGO}_M - \mathrm{RGO})/5000 \\ &\text{IF RGO} \leq \mathrm{RGO}_M - 5000\text{: } K_{\mathrm{dsm}} = 1 \end{aligned} \tag{3}$$

RGO_M is the range-to-go specified by the designer at which the energy management is ramped down and the homing element begins to become active in the *x*-*z* plane of the *P* frame.

The value of RGO_M is a function of the range from the launch point to the target.

$$\mathrm{RGO}_M = \mathrm{RGO}_{M\mathrm{slope}}(R_t - R_{\max}) + \mathrm{RGO}_{M\max} \tag{4}$$

$\mathrm{RGO}_{M\mathrm{slope}}$ is the desired slope of RGO_M with target range (unitless). $\mathrm{RGO}_{M\max}$ is the value of RGO_M at $R_{\max}$ (in feet). R_t is the target total

range from the projectile launch point (in feet). $R_{\max}$ is the maximum guided range of the projectile (in feet)

The value of RGO_M is typically negative so that the fraction of the flight dedicated to homing control decreases as the total flight range increases. This ensures that the energy management provides a larger fraction of the flight as the range extends. This allows for maximum range extension through careful energy management, but provides increased trajectory control at the shorter ranges where energy management is not important.

III. Homing Component

The homing guidance algorithm steers the missile to the desired final aimpoint (in NEDL coordinates) and to a desired final velocity orientation relative to the NEDL coordinates. For short range missions, where the flat Earth model may be assumed, the dispense flight-path angle relative to the local horizon is the same as the flight-path angle relative to the NEDL frame. Similarly, the commanded final azimuthal angle is the same in the NEDL coordinates and the local North, East, down coordinates at the target location. For longer range missions, where spherical Earth effects are important, a correction may be needed.

The homing guidance acceleration is normal to the velocity vector because the uncontrolled portion along the velocity vector has been removed [15,17]. The azimuthal orientation of the final velocity is given by an optimized rule set based on the current bearing off of the line of sight to the target.

The homing guidance law is given by [15]:

$$\bar{a}_{\mathrm{exp}}^{\mathrm{NEDL}} = \frac{V^2}{\mathrm{RGO}}[C_1(\hat{r}^{\mathrm{NEDL}} - \cos\delta\hat{v}^{\mathrm{NEDL}}) + C_2(\hat{v}_f^{\mathrm{NEDL}} - \cos\mu\hat{v}^{\mathrm{NEDL}})] \tag{5}$$

where $\hat{r}^{\mathrm{NEDL}}$ is the unit vector for the line of sight to the target point expressed in NEDL coordinates; δ is the current heading error between the line of sight and the current velocity; $\hat{v}^{\mathrm{NEDL}}$ is the unit vector along the current velocity expressed in NEDL coordinates; $\hat{v}_f^{\mathrm{NEDL}}$ is the unit vector for the desired final velocity orientation; μ is the angle between the current velocity and the desired final velocity orientation; C_1, C_2 are the two explicit guidance gains; V is the missile speed (in feet per second); RGO is the range-to-go (in feet).

The azimuthal orientation of the final velocity is given by a rule set based on the current bearing off of the line of sight to the target. The azimuthal angle of the line of sight is given by the components of the line-of-sight unit vector.

$$\tan(\psi_{\mathrm{LOS}}) = \left(\frac{\hat{r}^{\mathrm{NEDL}}|_y}{\hat{r}^{\mathrm{NEDL}}|_x}\right) \tag{6}$$

where $\hat{r}^{\mathrm{NEDL}}$ is the direction vector along the line of sight from the projectile current position to the target point location.

The current value of the projectile velocity azimuth in the NEDL frame is determined from the components of the missile velocity in this frame.

$$\tan(\psi_M) = \left(\frac{\hat{v}^{\mathrm{NEDL}}|_y}{\hat{v}^{\mathrm{NEDL}}|_x}\right) \tag{7}$$

The commanded azimuth angle of the missile velocity in the NEDL frame at the final point is

$$\psi_f = \psi_{\mathrm{LOS}} - K_\psi(\psi_M - \psi_{\mathrm{LOS}}) \tag{8}$$

The value of K_ψ is set to a value between one and two. As is the common practice with the explicit algorithms, the value of the C_2 is set to zero near the intercept. For the current algorithm, this occurs at 10 s time-to-go.

The homing guidance is initiated once the flight-path angle during the initial ascent after launch drops below a value as determined by the parameter γ_P, which is the *Homing Guidance Start Flight-Path Angle* selected by the designer.

IV. Time-of-Flight Control Element

To satisfy the multiple simultaneous round requirement, the guidance algorithm may be enabled to control the absolute time of flight to the target point. Whereas the MSR requirement is specified as a relative time of arrival, the time-of-flight control is implemented in terms of the absolute time of flight because no communication occurs between projectiles in the salvo.

The second term considered in Eq. (2) is a composite bias term. The first element of the bias is the correction for the acceleration due to gravity $\bar{a}_{g\mathrm{bias}}^P$, which is not considered in the development of [15,17]. The second element $\bar{a}_{\mathrm{TOF}_{\mathrm{bias}}}^P$ is the additional bias added for time-of-flight control. The bias term is then defined by

$$\bar{a}_{\mathrm{bias}}^P = \bar{a}_{g\mathrm{bias}}^P + \bar{a}_{\mathrm{TOF}_{\mathrm{bias}}}^P \tag{9}$$

$$\bar{a}_{g\mathrm{bias}}^P = \begin{Bmatrix} 0 \\ 0 \\ -g' \end{Bmatrix} \tag{10}$$

where g' is the local acceleration due to gravity (in feet per second squared).

The time-of-flight bias is determined during the flight by the in-flight time-of-flight control algorithm. If the time-of-flight control algorithm is not invoked, then it is the null vector. If the time-of-flight algorithm is invoked, the form of the time-of-flight bias in the P frame is

$$\bar{a}_{\mathrm{TOF}_{\mathrm{bias}}}^P = \begin{Bmatrix} 0 \\ 0 \\ a_{\mathrm{TOF}_{\mathrm{bias}}} \end{Bmatrix} \tag{11}$$

The in-flight time-of-flight control corrects for factors unknown at launch. These factors include rocket motor variations, drag variations, and unknown winds.

The in-flight time-of-flight control depends on selection of the $a_{\mathrm{TOF}_{\mathrm{bias}}}$ that is computed as part of the guidance command. During time-of-flight control guidance, the value of $a_{\mathrm{TOF}_{\mathrm{bias}}}$ is updated iteratively with each guidance update based on the current predicted flight time to the target. The predicted flight time to the target is based on an onboard 3 degrees of freedom simulation of the projectile assuming a constant value of a $a_{\mathrm{TOF}_{\mathrm{bias}}}$ with the planned guidance algorithm for the remainder of the flight. This approach is a form of model predictive control.

To minimize the computational workload required for the MPC approach, it is desired to limit the number of trajectories that must be run. The global optimal for the open-loop control (in the present formulation, the acceleration bias) does not need to be determined at each MPC update to ensure stability. An iterative approach, in which the performance index (in the present paper, the magnitude of the error in the time of flight relative to the commanded value) is reduced in each iteration update, guarantees stability [28]. This thought leads to the present concept of the use of a slowly iterating approach that performs only one update (and trajectory simulation) at each MPC update.

To achieve feasibility of the solution, a hybrid approach is employed. In this hybrid approach, existing guidance algorithms are embedded in the MPC by the composite guidance law to ensure feasibility in terms of the final position and velocity orientation. A *stability constraint* is applied during time-of-flight control on the other elements of the composite guidance law. The stability constraint is an increase in the time-to-go at which the explicit gain C_2 is set to zero from the nominal 10–15 s. This stability constraint is selected so that the composite guidance is able to meet the mission inequality constraint that the vertical flight-path angle must be steeper than −60 deg, but it does prevent the guidance from achieving the commanded flight path of −70 deg used in the guidance design. Unfortunately, the selection of the value of the stability constraint with the MPC control continues to require simulation and Monte Carlo analysis to ensure acceptable behavior for implemented designs.

This onboard simulation is initialized by the current estimated missile states from the navigation algorithm and the simulation is called once per iteration. A 0.4 Hz update rate for the time-of-flight control bias provides sufficient control of the time of flight.

The difference of the current estimate of the time of flight for the current value of $a_{\mathrm{TOF_{bias}}}$ ($t_{\mathrm{predict}k}$) and the commanded time of flight (t_{command}) is the current time-of-flight error.

$$\Delta t_{\mathrm{err}k} = t_{\mathrm{predict}k} - t_{\mathrm{command}} \tag{12}$$

If the current time-of-flight error and the previous time-of-flight error ($\Delta t_{\mathrm{err}k-1}$) have different polarity, then their product f_1 will be negative.

$$f_1 = \Delta t_{\mathrm{err}k} \Delta t_{\mathrm{err}k-1} < 0 \tag{13}$$

For this case, the value of $a_{\mathrm{TOF_{bias}}}$ that zeros the time-of-flight error lies between the current value of $a_{\mathrm{TOF_{bias}}k}$ and the previous value of the bias $a_{\mathrm{TOF_{bias}}k-1}$. Thus, for the case of $f_1 < 1$, the next value of the bias is given by

$$a_{\mathrm{TOF_{bias}}k+1} = (a_{\mathrm{TOF_{bias}}k} + a_{\mathrm{TOF_{bias}}k-1})/2 \tag{14}$$

If the value of $f_1 > 0$, then both the current and the previous values of the time-of-flight bias lie on the same side of the value which will zero the time-of-flight error. For this case, the next value of the bias is changed based on the computed error $\Delta t_{\mathrm{err}k}$. In this case, the next iteration of the bias acceleration $a_{\mathrm{TOF_{bias}}k+1}$ is

$$a_{\mathrm{TOF_{bias}}k+1} = a_{\mathrm{TOF_{bias}}k} + k_t \Delta t_{\mathrm{err}k} \tag{15}$$

where k_t is a user selectable gain nominally set to a value of one.

The basis for this update algorithm is that increased positive (i.e., downward) bias decreases the flight time to the target. If the predicted time of flight is short ($\Delta t_{\mathrm{err}k} < 0$), then the algorithm makes the bias more negative (upward) to slow the flight.

Finally, the value of $a_{\mathrm{TOF_{bias}}}$ is limited. It can be no less than -96.6 ft/s^2 and no greater than 32.2 ft/s^2. Little time-of-flight control is available for values of $a_{\mathrm{TOF_{bias}}}$ between 0 and 32.2 ft/s^2.

The initial value of $a_{\mathrm{TOF_{bias}}}$ is nominally set to the value of -32.2 ft/s^2 but the rapid convergence of the algorithm makes the performance of the time-of-flight controller insensitive to the initial value.

V. Energy Management

The third component of the algorithm in Eq. (2) is the energy management term. The term is designed to fly the missile along an energy-conserving trajectory by establishing a maximum L/D glide path with flight-path angle model following. During the ascent, the energy management term generates no acceleration command until the flight-path angle is less than the *glide guidance start angle* γ_{GL}.

The energy management term is best defined in the P frame because it represents management of the vertical shaping. In the P frame, the bias term is given by

$$\bar{a}^{\,P}_{\mathrm{EM}} = \begin{Bmatrix} 0 \\ 0 \\ a^* \end{Bmatrix} \tag{16}$$

The scalar commanded acceleration a^* is computed by a controller which seeks to place the missile at the maximum L/D subject to the flight-path angle follower.

$$a^* = C_L^* q S_{\mathrm{ref}}/W \tag{17}$$

$$C_L^* = \tilde{C}_L + k_\gamma(\gamma^* - \gamma) \tag{18}$$

where γ is the current flight-path angle, γ^* is the commanded flight-path angle, $\tilde{C}_L$ is the lift coefficient for maximum lift-to-drag ratio, C_L^* is the commanded lift coefficient for energy management, k_γ is the gain used to control stiffness of the flight-path angle model follower, q is the current dynamic pressure (in pounds per feet squared), S_{ref} is the aerodynamic reference area (in square feet), and W is the weight of the projectile (in pounds). The flight-path follower can be used to eliminate the phugoid mode of gliding vehicles excited when the glider is launched on its gliding trajectory at an altitude that does not allow for an equilibrium glide at the desired maximum lift-to-drag ratio.

The anticipated energy loss during the glide is used compute the glide slope to ensure constant dynamic pressure. From [23], the equation for the commanded flight-path angle γ^* is

$$\gamma^* = \frac{1}{(L/D)_{\max}|1 + \beta(V^2/2g)|} \tag{19}$$

where $(L/D)_{\max}$ is the maximum lift-to-drag ratio for the projectile at the current conditions, β is the exponential atmosphere density exponent, and g is reference acceleration due to gravity (32.2 ft/s^2).

VI. Fire Control for Multiple Simultaneous Round Time-of-Flight Control

The time-of-flight control is performed by two distinct algorithms during prelaunch and in-flight. During the prelaunch phase, the goal is to create planned trajectories of varying time-to-target values to account for the delayed launches of the remaining rounds in the salvo. The maximum rate of fire of the gun is known and thus the amount of time-of-flight variation to be planned for each round in the salvo is known. The prelaunch phase is concerned with controlling the relative time of flight of the rounds in the salvo. No requirement exists on the salvo absolute time of arrival.

In the prelaunch time-of-flight control, the first round is fired along a planned trajectory with the slowest time of flight to the target. For a gun that is capable of firing a round every 5 s, the second round in the salvo is then fired along a trajectory which is 5 s faster than the first trajectory. The third round is then fired along a trajectory that is 10 s faster than the slowest trajectory. The process continues until the salvo is complete or the maximum time-of-flight flexibility has been achieved.

The variation in the planned time-of-flight control is achieved by varying the elevation and azimuth angle of the barrel at firing. The azimuth angle varies from 0 deg for the minimal elevation angle up to the maximum azimuth value for the maximum elevation angle. The longest flight times are achieved with the highest barrel elevations and largest azimuth angles.

For the prediction of the time of flight for the prelaunch phase, all round conditions are held at their nominal values. For time-of-flight control guidance, the nominal value of the time-of-flight control acceleration bias $a_{\mathrm{TOF_{bias}}}$ is -32.2 ft/s^2. This value is necessary to give the in-flight time-of-flight control algorithm adequate control authority.

VII. Results

The guidance algorithm was exercised with and without the time-of-flight control activated in a 3-degree-of-freedom flat Earth model with a 1962 Standard Atmosphere[‡] and an inverse square gravity model. The requirements placed on the guidance algorithm are given in Table 1. The trajectories were run with the guidance parameters in Table 2 unless otherwise noted.

Figure 2 presents the family of trajectories produced by the composite guidance algorithm for a range of in-plane target points. The projectile is commanded to arrive with a commanded final flight-path angle at the target of 70 deg below the local horizon. The projectile is launched at a 60 deg barrel angle at an exit speed of 2800 ft/s. The point to which the projectile is guided is fixed. The final time of flight and the final speed are indicated in the figure. The lower apogees for the shorter range target points are created by the greater range-to-go for transition to the homing guidance as the target

[‡]U.S. Standard Atmosphere, U.S. Government Printing Office, Washington, D.C., 1962.

Table 1 Guidance algorithm constraints

Parameter	Constraint
Final flight-path angle	< -60 deg
Perfect targeting miss distance	<0.1 ft
Relative time-of-arrival	<2 s

range decreases. Essentially, the projectile begins to respond to the homing commands during the ascent as soon as the command-start flight-path angle is reached and begins to pull down to the desired target point and flight-path angle. For these intercepts, the energy management algorithm is not activated. Figure 3 shows the speed histories for these trajectories where the postlaunch rocket motor firing is clearly visible. The energy management proportion of the trajectory increases with range. For a range less than 40 n miles, the energy management algorithm does not play a significant role in the flight. Beyond 40 n miles, the energy management algorithm provides the initial phase of the guidance and does not produce acceleration commands until the apogee is reached. For the 50 n mile intercept, the homing algorithm does not contribute until 270 s into the flight.

Figure 4 shows the relationship between the achieved flight-path angle and the desired optimal flight-path angle from the energy management algorithm for the 50 n mile target point trajectory. After the initial pull-up from the apogee, the energy management algorithm commands cause the flight-path angle to oscillate about the optimal value. The amplitude of the oscillation can be controlled by selection of the values of k_γ. Then, the homing guidance pulls down the flight path to meet the specified end constraints for zero miss distance and flight-path angle. The miss distances for these fixed target points are within the accuracy of the simulation and the achieved flight-path angles are within 7 deg of the commanded 70 deg below the local horizon.

An important feature of the guidance algorithm is its performance against moving targets. Figure 5 shows the projectile trajectory against a tanklike target that is initially at rest at 43 n miles downrange from the launch point, and which begins to move normal to the launch bearing immediately after launch. The target vehicle accelerates along its direction of travel at 10 ft/s^2 until it achieves a speed of 88 ft/s^2. After this point, the target vehicle continues to move at a constant speed and bearing. An offboard targeting system provides perfect target coordinates which are passed through an alpha-beta filter with values of $\alpha = 0.4$ and $\beta = 0.1$ and an update rate of 20 Hz. The projectile flies to the predicted intercept point using the inferred velocity from the filter and the time of flight to the intercept from an onboard trajectory simulation updated at 2 Hz. There is no delay on transmission on the target coordinates. The intercept occurs at 43.0 n miles downrange and 3.5 n miles crossrange with a time of flight of 246 s. The commanded flight-path angle was -70.0 deg and the achieved flight path was -66.6 deg. The guidance algorithm selects a commanded azimuth angle based on the intercept geometry and achieves a final value of 22.0 deg. The achieved miss distance is within the accuracy of the simulation.

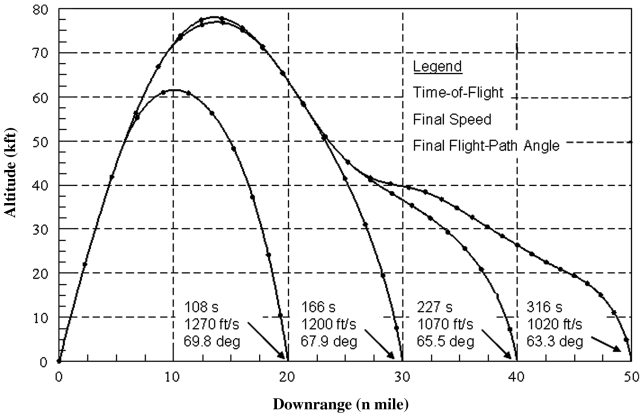

Fig. 2 Composite guidance trajectories.

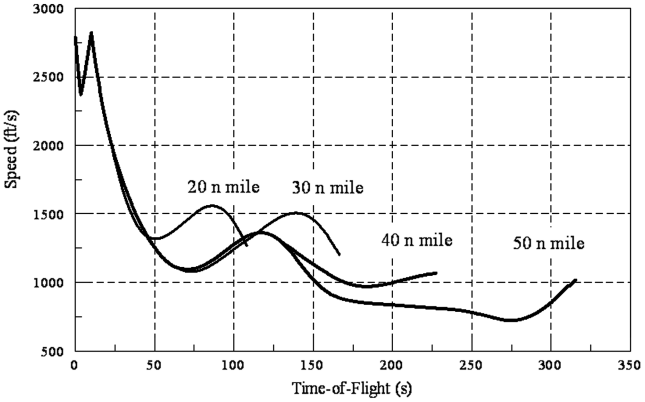

Fig. 3 Speed histories.

The performance of the algorithm without the time-of-fight control under targeting noise was considered. As before, targeting is provided by an offboard targeting system, which provides a stationary white noise process error on the target coordinates in the downrange and crossrange coordinates. Table 3 presents the miss distance in the downrange and crossrange directions as a function of the targeting error. The resulting miss distances are consistent with the expected out-to-input noise variance for the predicted position for the alpha-beta filter and tend to essentially zero as the targeting noise goes to zero. The guidance algorithm behaves in a stable, well-mannered fashion in response to targeting noise.

The prelaunch time-of-flight fire control performance was evaluated. The elevation angle is varied from 60 to 65 deg, and the barrel azimuth angle off of the line of sight to the target is scheduled linearly with barrel elevation to a maximum value of 25 deg off of the line of sight to the target. The resulting time-of-flight windows that may be achieved with the barrel elevation and azimuthal angle

Table 2 Guidance design parameters

Guidance parameter	Value
$\text{RGO}_{M_{\text{slope}}}$	-1, unitless
$R_{\max}$	3.281×10^5, ft
$\text{RGO}_{M_{\max}}$	5.7×10^4, ft
C_1	6
C_2	-2
Onboard time-of flight model update rate	0.4 Hz
k_γ	0.25
k_ψ	2
γ_p homing guidance start flight-path angle	35 deg, $R_t \geq 30$ n mile 35–50 deg, $20 \leq R_t \leq 30$ n mile 50 deg, $R_t \leq 20$ n mile
γ_{GL} energy management start flight-path angle	0 deg

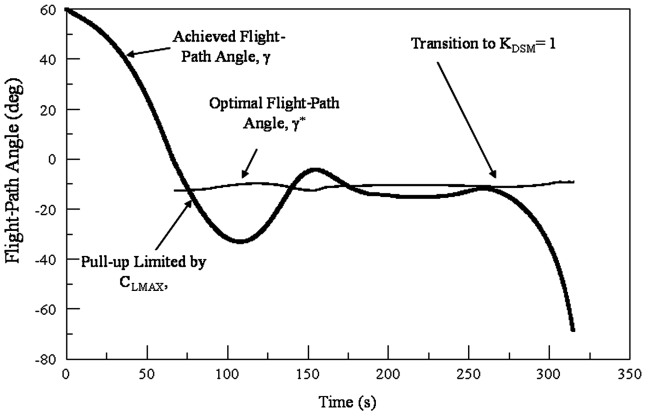

Fig. 4 Fifty nautical mile trajectory flight-path angle.

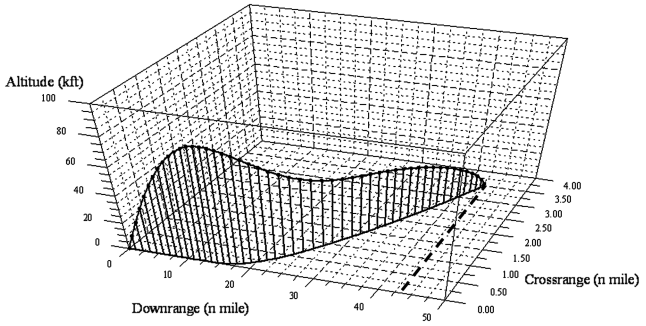

Fig. 5 Crossrange moving target intercept.

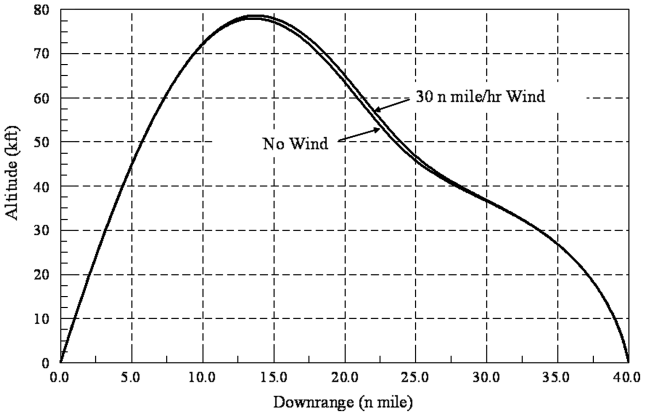

Fig. 6 Effect of wind on nominal guidance.

selections are shown in Table 4. Thus, by selection of these two parameters, the simultaneous time of arrival may be planned for up to eight rounds with a launch dwell time of 5 s. The selection of the two angles must be such that the gun slew time does not exceed the gun dwell time.

The effect of in-flight conditions on the time-of-flight variation for the non-time-of-flight guidance algorithm illustrates the need for the in-flight time-of-flight algorithm. A trajectory against a fixed target location with no targeting noise, but with a deterministic variation in the wind, was considered. The only variation source in the simulation was a constant 30 n mile tailwind which was not known before launch. Thus, the tailwind is not considered in the fire control solution. Figure 6 shows the resulting trajectories and time of flight. Although the trajectory variation appears relatively minor, the time of flight varies by approximately 9 s, which is greater than is permissible for satisfactory lethality performance.

Table 4 Prelaunch time-of-flight control windows

Range, n mile	Q_E, deg	ψ_i, deg	ToF, s	Window, s
20	60	0	175.1	
20	65	25	212.4	37.3
30	60	0	177.2	
30	65	25	218.5	41.3
40	60	0	247.4	
40	65	25	284.0	36.6
50	60	0	324.8	
50	65	25	370.7	45.9

To correct for these unknown in-flight variations, the in-flight time-of-flight control algorithm must be activated. First, a deterministic ± 100 ft/s variation in the muzzle exit velocity is considered. Figure 7 shows the three trajectories with the in-flight time-of-flight controller active for a commanded total time of flight from the launch of the first round of 248.5 s. The fast muzzle exit velocity of 2900 ft/s results in an increase in the bias magnitude and a higher trajectory. The higher trajectory slows the average groundspeed of the projectile to correct for the greater initial speed. Figure 8 shows the history of the time-of-flight commanded bias for the three trajectories. The rapid convergence of the bias and its stability are readily apparent. Unfortunately, the use of the bias as the control mechanism for the in-flight time-of-flight control algorithm leads to a disruption in the achieved final flight-path angle. Table 5 presents the achieved final flight-path angle for these three trajectories. It should be noted that the 2900 ft/s trajectory is coming in at an azimuth of -180 deg (inbound along the radial from the launch point to the target point) at the target point. The 2900 ft/s launch speed trajectory has an increased final speed reflecting the increased energy provided by the launch into the projectile. It should be noted that the nominal 2800 ft/s launch speed trajectory has an increased speed compared with the non-time-of-flight control trajectory. This indicates that the increased performance may be obtained beyond the explicit guidance algorithm [17] with the nominal gains.

The second example is a steady 30 kt wind that is unknown to the fire control system. This wind is present immediately after launch and persists through the impact at the target. Its magnitude and direction (tailwind) are constant throughout the flight. Because the wind velocity is unknown to the fire control, the commanded time of flight from the fire control will be longer than the trajectory would be without the in-flight controller. Figure 9 shows the time-of-flight control guidance trajectory without the unknown wind and with the unknown wind. The rapid convergence of the commanded bias is evident from the commanded bias history in Fig. 10.

The achieved flight-path angle is -83.0 deg without the tailwind and -67.1 deg with an azimuth angle of -180 deg (inbound) with the tailwind. Both trajectories impacted the target at the commanded time of 248.5 s.

The two results for the time-of-flight control guidance were based on perfect knowledge of the launch speed variation and the current wind speed. For variations unknown before launch, but which are directly observable by instruments aboard the projectile, this is a

Table 3 Miss performance in the presence of targeting noise

Downrange noise 1σ, ft	Crossrange noise 1σ, ft	Downrange miss 1σ, ft	Crossrange miss 1σ, ft
0.0	0.0	0.0	0.0
3.0	3.0	2.4	2.6
6.0	6.0	10.1	3.8

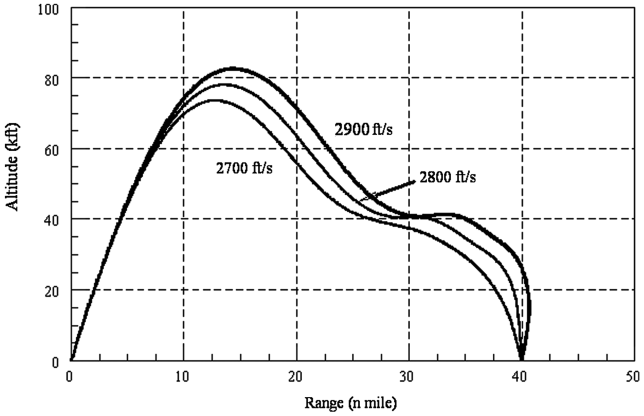

Fig. 7 In-flight ToF control compensates for variable gun exit speed.

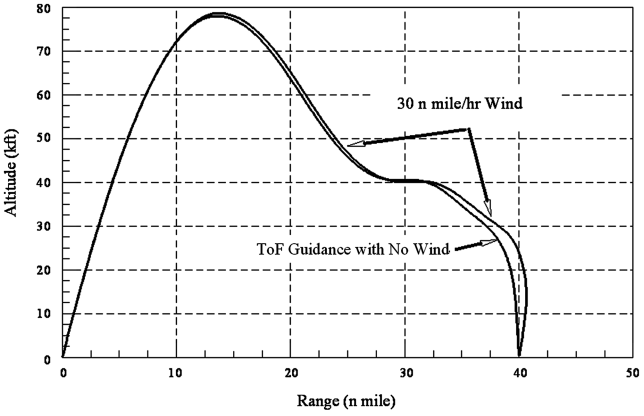

Fig. 9 In-flight ToF guidance counteracts unknown wind.

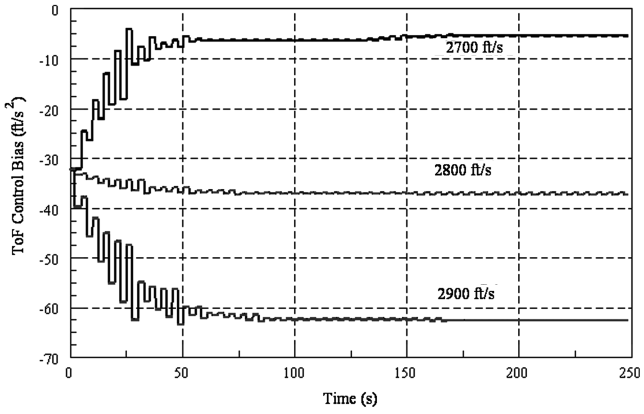

Fig. 8 ToF control bias algorithm converges quickly.

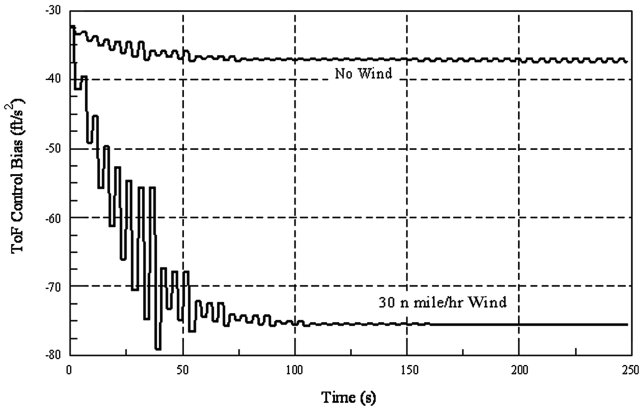

Fig. 10 ToF control bias converges quickly for wind.

good assumption. For quantities that must be inferred indirectly from measurements, such as wind or vehicle aerodynamic coefficients, there will be degradation in absolute time of flight and multiple round relative flight control due to errors in the estimates. The requirement for the algorithm is to bring multiple projectiles to bear on the target within a specified time ($\sim$2 s) and not on the absolute time of flight. Therefore, variations and uncertainties that bear on all of the rounds in a salvo may not directly impact the relative time of arrival but will impact it through secondary effects. Thus, any variations associated with the meteorological day assumed in the prelaunch phase will bear on all rounds equally and will not have a major impact on the relative time of arrival on the salvo. Items that will vary round-to-round will have an impact on the relative arrival.

The following vehicle parameter uncertainties will affect the relative performance: the normal force coefficient slope $C_{N\alpha}$, the maximum normal force coefficient $C_{N\max}$, the axial force coefficient C_A, and the wind speed along the different paths to the target. The projectile may use an estimation algorithm to estimate the values of these parameters. For this case, it is the residual errors from these algorithms that drive the width of the time-of-arrival envelope. The uncertainty in these parameters, multiplied by their sensitivity, will determine the width of the arrival window at the target. Table 6 presents the sensitivity of the algorithm error in delivering the projectile to the target at the commanded time for each of these error sources. In this table, the uncertainties are treated as constant bias errors present through the entire flight. Thus, if the uncertainties represent the maximum value of a time-varying parameter, the impact on the achieved time-of-flight accuracy will be lessened, as they will tend to a smaller average value over the flight. Also, any error in the aerodynamic parameters that is true for the entire population of projectiles would not impact this calculation.

VIII. Conclusions

A composite guidance algorithm combining the near-equilibrium glide management algorithm for energy management, the vectorized three-dimensional version of the explicit algorithm, and a model process control approach for the in-flight control of time-of-flight has been presented. When the time-of-flight algorithm is not active, the algorithm achieves zero miss and the desired tolerance of the flight-path angle for zero noise targeting. The ability to target moving and

Table 6 ToF control sensitivities

Parameter	Absolute time-of-flight error sensitivity
$C_{N\alpha}$	0.3 s/(%uncertainty of $C_{N\alpha}$)
C_A	0.5 s/(%uncertainty of C_A)
C_N	0.1 s/(%uncertainty of C_N)
Downrange wind estimate	0.05 s/(ft/s error in wind estimate)

Table 5 Final conditions for ToF control trajectories

Gun exit speed, ft/s	Time of flight, s	Final speed, ft/s	Final flight-path angle, deg
2700	248.5	1073	−63
2800	248.5	1093	−83
2900	248.5	1145	−69

crossing targets was demonstrated. The composite algorithm retains the performance of the original explicit guidance algorithm in the presence of targeting noise. A method to allow multiple simultaneous round impact for a boost glide vehicle was demonstrated by means of prelaunch variation in the trajectory shaping for the known delay in firing of multiple rounds because of the gun launch rate and an in-flight time-of-flight algorithm, based on an onboard model predictive control approach. The use of the bias in the composite algorithm as a control for the time-of-flight control leads to a disruption of the achieved final flight-path angle but the mission requirements on the final flight-path angle can be satisfied. The model predictive control at a reasonable update rate (0.4 Hz) was demonstrated to be sufficiently fast to control the slowly varying time-of-flight dynamics against fixed targets. Stability of MPC algorithms remains a concern because heuristically developed stability constraints are added to elements of the composite guidance algorithm to ensure proper behavior of the time-of-flight control. The development of these stability constraints requires the use of simulation and Monte Carlo analysis to ensure proper behavior of a deployed system.

Appendix: Vehicle Aerodynamic Model

The vehicle used in the current analysis is a generic diameter projectile with canard control and fixed tail fins. After gun launch, a rocket motor is fired to increase the energy of the vehicle. The aerodynamic features are modeled as a trim aerodynamic model. Under this assumption, the axial force is modeled as being composed of five terms. The first, C_{A00}, is the axial force coefficient for sea level as a function of Mach number. The second term $C_{A\alpha}$ is the correction for total angle of attack as a function of the Mach number. The third term C_{AMh} is the correction for altitude as a function of Mach number and altitude. The fourth term C_{AT} is a correction for the effect of thrust on the base drag contributions as a function of Mach number, and the fifth term $C_{A\delta}$ is the axial force correction for the period before canard deployment as a function of Mach number. The axial force model is given in Eq. (A1).

$$C_{A0} = C_{A00}(M) + C_{A\alpha}(M, \alpha_T) + C_{AMh}(M, h) + C_{AT}(M) + C_{A\delta}(M) \tag{A1}$$

The normal force model consists of the normal force slope $C_{N\alpha}$ and maximum normal force coefficient $C_{N\max}$. Both are modeled as a function of the Mach number.

The maximum lift-to-drag ratio is then computed using the standard relations. The maximum lift-to-drag ratio for the projectile at sea level with the canards deployed and the rocket motor burned out is given in Fig. A1. The zero-lift ballistic coefficient at sea level with the canards deployed is given in Fig. A2, where the ballistic coefficient B is given by

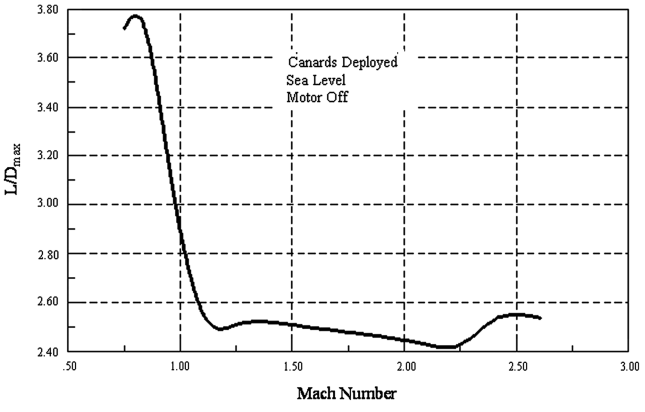

Fig. A1 Maximum L/D ratio.

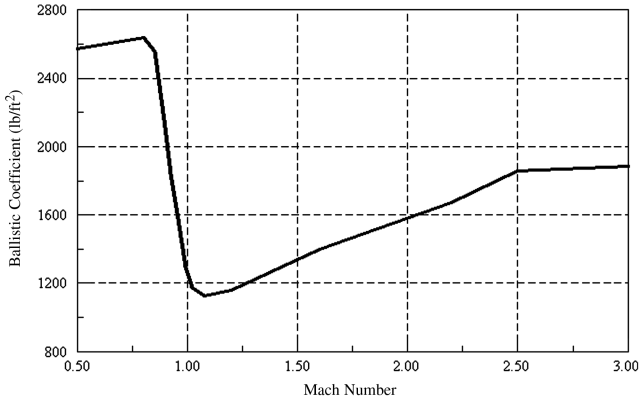

Fig. A2 Zero-lift ballistic coefficient at sea level.

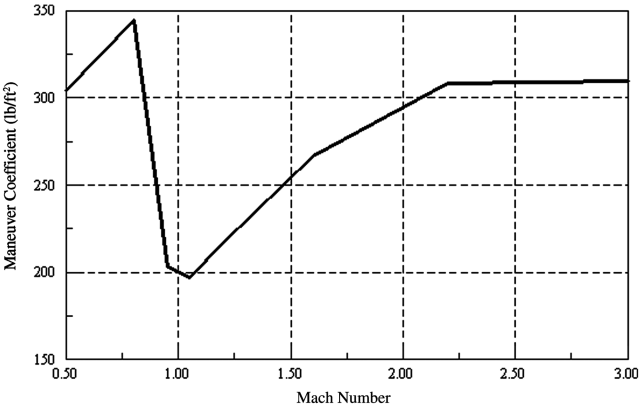

Fig. A3 Maneuver coefficient.

$$B = W/(C_A S_{\text{ref}}) \tag{A2}$$

The maximum maneuver capability of the round is given by the maneuver coefficient in Fig. A3. The maneuver coefficient M is given by

$$M = W/(C_{N_{\max}} S_{\text{ref}}) \tag{A3}$$

Acknowledgments

The author appreciates the contributions of D. Stephen Malyevac of the Naval Surface Warfare Center who was instrumental in the development of this guidance law. The Associate Editor, Michael McFarland, and the reviewers provided many insightful comments to greatly improve the paper. These algorithms are protected under two U.S. Patents: Patent # 6,676,071 B1 *Gliding Vehicle Guidance*, 13 Jan. 2004 and Patent # 6,776,369 B2 *Gliding Vehicle Guidance*, 17 Aug. 2004.

References

[1] Morrison, P. H., and Amgernstont, D. S., "Guidance and Control of a Cannon-Launched Guided Projectile," *Journal of Spacecraft and Rockets*, Vol. 14, No. 6, 1977, pp. 328–334. doi:10.2514/3.57205

[2] Adler, P., "Missile Guidance by Three-Dimensional Proportional Navigation," *Journal of Applied Physics*, Vol. 27, No. 5, 1956, pp. 500–507. doi:10.1063/1.1722411

[3] Nesline, F. W., and Zarchan, P.,"New Look at Classical vs Modern Homing Missile Guidance," *Journal of Guidance, Control, and Dynamics*, Vol. 4, No. 1, 1981, pp. 78–85. doi:10.2514/3.56054

[4] Nesline, F. W., and Zarchan, P.,"Miss Distance Dynamics in Homing Missiles," *Proceedings of the AIAA Guidance Navigation, and Control Conference*, AIAA Paper 84-1844, Aug. 1984.

[5] Chadwick, W. R., "Miss Distance of Proportional Navigation Missile with Varying Velocity," *Journal of Guidance, Control, and Dynamics*, Vol. 8, No. 5, 1985, pp. 662–666. doi:10.2514/3.20038

[6] Murtaugh, S. A., and Criel, H. E., "Fundamentals of Proportional Guidance," *IEEE Spectrum*, Vol. 3, No. 6, Dec. 1966, pp. 75–85.

[7] Cherry, G., "General Explicit, Optimizing Guidance Law for Rocket-Propelled Spacecraft," AIAA Paper 64-638, Aug. 1964.

[8] Lin, C. F., *Modern Navigation, Guidance, and Control Processing*, Prentice–Hall, Englewood Cliffs, NJ, 1991, Sec. 8.6.

[9] Zarchan, P., "*Tactical and Strategic Missile Guidance*," 4th ed., Vol. 199, Progress in Astronautics and Aeronautics, AIAA, Reston, VA, 2002, Chap. 25.

[10] Kim, M., and Grider, K. V., "Terminal Guidance for Impact Attitude Angle Constrained Flight Trajectories," *IEEE Transactions on Aerospace and Electronic Systems*, Vol. aes-9, No. 6, 1973, pp. 852–859. doi:10.1109/TAES.1973.309659

[11] Kim, B. S., Lee, G. L., and Han, H. S., "Biased PNG Law for Impact with Angular Constraint," *IEEE Transactions on Aerospace and Electronic Systems*, Vol. 34, No. 1, 1998, pp. 277–288. doi:10.1109/7.640285

[12] Song, T. L., and Shin, J. S., "Time Optimal Impact Angle Control for Vertical Plane Engagements," *IEEE Transactions on Aerospace and Electronic Systems*, Vol. 35, No. 2, 1999, pp. 738–742. doi:10.1109/7.766954

[13] Song, T. L., Shin, J. S., and Han, H. S., "Impact Angle Control for Planar Engagements," *IEEE Transactions on Aerospace and Electronic Systems*, Vol. 35, No. 4, 1999, pp. 1439–1444. doi:10.1109/7.805460

[14] Manchester, I. R., and Savkin, A. V., "Circular Navigation Guidance Law for Precision Missile Target Engagements," *Proceedings of the 41st IEEE Conference on Decision and Control*, Vol. 2, Inst. of Electrical and Electronics Engineers, Piscataway, NJ, 2002, pp. 1287–1292.

[15] Ohlmeyer, E. J., "Control of Terminal Engagement Geometry Using Generalized Vector Explicit Guidance," *Proceedings of American Control Conference*, Vol. 1, Inst. of Electrical and Electronics Engineers, Piscataway, NJ, 2003, pp. 396–401.

[16] Manchester, I. R., and Savkin, A. V., "Circular Navigation Missile Guidance with Incomplete Information and Uncertain Autopilot Model," *Journal of Guidance, Control, and Dynamics*, Vol. 27, No. 6, 2004, pp. 1078–1083. doi:10.2514/1.3371

[17] Ohlmeyer, E., and Phillips, C., "Generalized Vector Explicit Guidance," *Journal of Guidance, Control, and Dynamics*, Vol. 29, No. 2, 2006, pp. 261–268. doi:10.2514/1.14956

[18] Savkin, A. V., Pathirana, P., and Faruqi, F. A., "Problem of Precision Missile Guidance: LQR and $H\infty$ Frameworks," *IEEE Transactions on Aerospace and Electronic Systems*, Vol. 39, No. 3, 2003, pp. 901–910. doi:10.1109/TAES.2003.1238744

[19] Bryson, A. E., and Ho, Y.-C., *Applied Optimal Control*, 1st ed., Blaisdell, Waltham, MA, 1969, pp. 60–61.

[20] Krieger, R. J., "Supersonic Missile Aerodynamic and Performance Relationships for Long-Range Mission Profiles," *Journal of Spacecraft and Rockets*, Vol. 21, No. 3, 1984, pp. 234–240. doi:10.2514/3.25643

[21] Wingrove, R. C., "Trajectory Control Problems in Planetary Entry of Manned Vehicles," *Journal of Spacecraft and Rockets*, Vol. 2, No. 6, 1965, pp. 883–888. doi:10.2514/3.28308

[22] Dewell, L. D., and Speyer, J. L., "Fuel-Optimal Periodic Control and Regulation in Constrained Hypersonic Flight," *Journal of Guidance, Control, and Dynamics*, Vol. 20, No. 5, 1997, pp. 923–932.

[23] Kelley, H. J., Clff, E. M., and Lutze, F. H., "Boost-Glide Range-Optimal Guidance," *Optimal Control Applications and Methods*, Vol. 3, No. 3, 1982, pp. 293–298.

[24] Lu, P., "Asymptotic Analysis of Quasi-Equilibrium Glide in Lifting Entry Flight," *Journal of Guidance, Control, and Dynamics*, Vol. 29, No. 3, 2006, pp. 662–670. doi:10.2514/1.15789

[25] Naidu, N. S., and Calise, A. J., "Singular Perturbations and Time Scales in Guidance and Control of Aerospace Systems: A Survey," *Journal of Guidance, Control, and Dynamics*, Vol. 24, No. 6, 2001, pp. 1057–1078.

[26] Schierman, J. D., Ward, D. G., Monaco, J. F., and Hull, J. R., "Reconfigurable Guidance Approach for Reusable Launch Vehicles," AIAA Paper 2001-4429, Aug. 2001.

[27] Slegers, N., and Costello, M., "Model Predictive Control of a Parafoil and Payload System," *Journal of Guidance, Control, and Dynamics*, Vol. 28, No. 4, 2005, pp. 816–821. doi:10.2514/1.12251

[28] Scokaert, P. O. M., Mayne, D. Q., and Rawlings, J. B., "Suboptimal Model Predictive Control (Feasibility Implies Stability)," *IEEE Transactions on Automatic Control*, Vol. 44, No. 3, 1999, pp. 648–654. doi:10.1109/9.751369